Enabling Higher Performance Concentric Tube Robots Via Multiple Constant-Curvature Tubes

Alex Lu[1], Felipe Ramos[2], Jui-Te Lin[2], Tania K. Morimoto[3]

***Abstract*— Concentric tube robots (CTRs) consist of a set of telescoping, pre-curved tubes, whose overall shape can be actively controlled by translating and rotating the tubes with respect to each other. The majority of CTRs to date consist of piecewise constant-curvature tubes, with a straight section followed by a single constant-curvature section. Several approaches have been proposed for CTR designs that can lead to improvements in metrics such as the workspace, orientability, dexterity, and stability. Here we propose to use CTRs with multiple constant-curvature sections. We perform two simulation studies that compare the performance of the multiple constant-curvature CTRs with standard single constant-curvature tubes. We also demonstrate how using one of the proposed multiple constant-curvature designs can enable the reduction in the number of tubes needed to achieve the same performance as a standard three-tube CTR.**

I. INTRODUCTION

Concentric tube robots (CTRs) consist of a set of superelastic, pre-curved tubes that are assembled concentrically, one inside the next [1], [2]. CTRs have $2n$ degrees of freedom in actuation space, including the translation and rotation of each tube, where n is the number of tubes [1]. The bending and torsional interactions between the tubes enable the robot body to achieve complex 3D shapes that can be actively controlled to navigate through constrained anatomy to perform surgical tasks [2]. The innermost tube can serve as an access channel for various types of end-effectors and tools. These capabilities, along with their small size (1-3 mm), make them well-suited for various minimally invasive surgical procedures [3], [4].

The tube architecture for standard CTRs consists of a straight section followed by a single constant-curvature section (SCC) towards the distal end. As the tubes are translated relative to each other, sections of the robot will consist of a varying number of overlapping tubes, each with their own individual pre-curvature. As a result, many of the performance metrics (e.g. workspace size, dexterity, orientability, and stability) by which a CTR is evaluated, are highly dependent on the design of these curved sections. In this paper, we propose to create tubes with sections of multiple constant curvature (MCC) (Fig. 1) in order to increase the performance of CTRs.

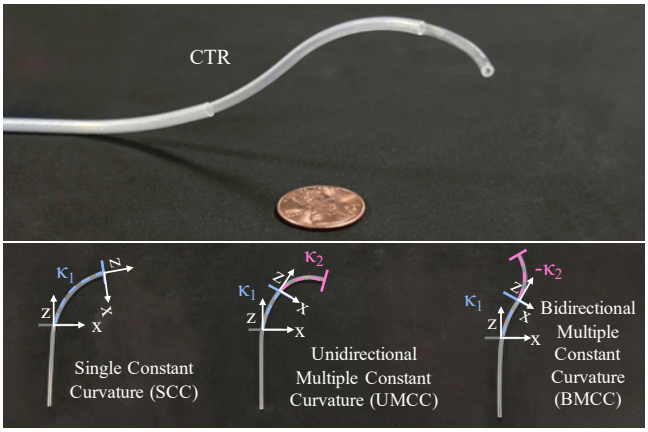

Fig. 1. Three-tube, nylon concentric tube robot (CTR) with multiple constant-curvature tubes (top). Examples of the standard single constant-curvature tube (SCC), along with the proposed unidirectional multiple constant-curvature (UMCC) tubes and bidirectional multiple constant-curvature (BMCC) tubes.

A. CTR Design

Several approaches have been proposed for CTR designs that can lead to improvements in the various performance metrics compared to what can be achieved using single constant-curvature tubes. For instance, in order to increase both the workspace of a CTR and its orientability, it has been shown that one can increase the number of variable-curvature, telescoping sections [5]. It has also been shown that integrating additional actuators — in particular magnets — into the tubes to actively change their curvature, can also lead to improvements in these same metrics [6], [7]. In addition, there have been numerous approaches proposed for increasing CTR stability. The simplest approach has been to use a stiffer material, such as stainless steel, for the transmission section. Another approach has been to pattern the tubes to reduce the ratio of bending to torsional stiffness, and therefore increase the overall stability [8]. Finally, it has been shown that using piecewise straight tubes [9] or using tubes with exponentially varying curvature [10] can also lead to an increase in the stability of the robot.

B. CTR Fabrication

To date, CTRs have primarily been made using Nitinol (NiTi) due to its superelastic property. In order to achieve the desired pre-curved shapes, Nitinol tubes must be heat-set, which typically requires specialized equipment to obtain

This work was supported in part by National Science Foundation grant 2146095.

[1]Alex Lu is with the Department of Bioengineering, University of California, San Diego, La Jolla, CA 92093 USA.

[2]Felipe Ramos and Jui-Te Lin are with the Department of Mechanical and Aerospace Engineering, University of California, San Diego, La Jolla, CA 92093 USA. Corresponding author: jul024@eng.ucsd.edu.

[3]Tania K. Morimoto is with the Department of Mechanical and Aerospace Engineering and the Department of Surgery, University of California, San Diego, La Jolla, CA 92093 USA.

consistent and accurate results [11]. The main method involves the use of a furnace, and can be quite inefficient, since it often requires significant trial and error to fine tune the settings [12]. In order to efficiently fabricate patient- or task-specific CTRs for different medical applications, alternative fabrication methods and new materials have been recently explored. One approach has been to instead use electric heating by passing a current through the Nitinol and causing the necessary increase in temperature [13]. This approach, although faster and more robust, can be challenging to properly tune and can suffer from uneven heating if the Nitinol tube is not fully constrained. Another approach has been to instead use 3D printing to create tubes made of various polymers [14], [15]. Such tubes, however, require higher wall thicknesses compared to Nitinol tubes, and the surface finish quality highly affects the amount of friction between the tubes. A final approach has been to heat set off-the-shelf extruded tubes, including those made of polyvinylidene fluoride (PVDF) or nylon [16], [17]. Despite the more rapid fatigue seen with the use of such plastic tubes, their improved visibility under MRI [17], combined with the ease of fabrication, make them a promising alternative.

C. Contributions

The contributions of this paper are as follows. First, we design and fabricate multiple constant-curvature (MCC) tubes, either with curvatures all in the same direction (unidirectional multiple constant-curvature tubes) or curvatures in alternating directions (bidirectional multiple constant-curvature tubes). Second, we present the evaluation and comparison of the performance of MCC tubes versus standard single constant-curvature tubes, illustrating both the advantages and trade-offs associated with these new tube architectures. Third, we demonstrate the feasibility of using fewer MCC tubes to achieve similar performance to a standard CTR design, which can enable less complicated overall systems. Finally, we demonstrate the first fully Nylon CTR with dimensions comparable to a standard Nitinol tube set.

II. TUBE DESIGN

In this section, the new MCC tube architectures are presented. An overview of the kinematics of a CTR are then provided, along with the methods used to compute a set of performance metrics (workspace, orientability, stability and dexterity) that will be used to compare the various designs.

A. CTR Design and Kinematics

The proposed unidirectional multiple constant curvature (UMCC) and bidirectional multiple constant curvature (BMCC) tubes are shown in Fig. 1. For the UMCC tube design, there are at least two constant curvature sections that both face the same direction. For the BMCC tube design, there are again at least two constant curvature sections, but one is curved towards the positive x-direction and one is curved towards the negative x-direction, as shown in Fig. 1. Since the tubes are piecewise constant curvature and planar, constructing the kinematic model for these tube architectures is the same as for the standard architecture (straight section followed by a single constant curvature section), but with additional planar curved sections. The pre-curvature vector can be described as $u^* = [u_x \ 0 \ 0]^T$. Because the curved sections of UMCC tubes are all curved in the same direction (i.e. +x as shown in Fig. 1), the pre-curvature vectors will have the same sign. However, the curved sections of BMCC tubes have pre-curvature vectors that alternate signs (i.e. +x then -x).

The CTR kinematics model is based on the Cosserat rod theory that describes the twist along the centerline of the robot from the proximal end to the distal end. The two-point boundary-value problem that solves a set of differential equations describing the tube angle ψ_i along the body of the robot is as follows [18]:

$$\ddot{\psi}_i = \frac{k_{ib}}{k_{it}k_b} \sum_{j=1}^{n} k_{jb}\kappa_i\kappa_j \sin(\psi_i - \psi_j), \tag{1}$$

where k_{ib} is the bending stiffness of tube i, k_{it} is the torsional stiffness of tube i, k_b is $\sum_{i=1}^{n} k_{ib}$, and κ_i is the curvature of tube i. The boundary conditions are $\psi_i(0) = \alpha_i - \beta_i\dot{\psi}_i(0)$ at the proximal end and $\dot{\psi}_i(L_i + \beta_i) = 0$ at the distal end of tube i.

After solving for the tube angle ψ_i using Eq. (1) with the associated boundary conditions, two additional first order differential equations are needed to derive the rotation $\mathbf{R} \in SO(3)$ and the position $\mathbf{p} \in \mathbb{R}^3$ along the robot backbone. The two ODEs with their initial conditions are described in [18] as:

$$\begin{aligned} \dot{\mathbf{R}} &= \mathbf{R}\hat{\mathbf{u}}, \quad \mathbf{R}(0) = \mathbf{R}_z(\psi_1(0)) \\ \dot{\mathbf{p}} &= \mathbf{R}\mathbf{e}_3, \quad \mathbf{p}(0) = \begin{bmatrix} 0 & 0 & 0 \end{bmatrix}^T \end{aligned} \tag{2}$$

where $\mathbf{u} = \mathbf{K}^{-1} \sum_{i=1}^{n} \mathbf{K}_i(\mathbf{R}_{\psi_i}\mathbf{u}_i^* - \dot{\psi}_i\mathbf{e}_3)$ is the curvature vector, $\mathbf{e}_3$ is the standard unit vector in the z-direction, $\mathbf{K}_i$ is the stiffness tensor, $\mathbf{K}$ is $\sum_{i=1}^{n} \mathbf{K}_i$, $\mathbf{R}_{\psi_i}$ is the rotation matrix about the z-axis by ψ_i, $\mathbf{u}_i^*$is the precurvature vector of tube i, $\mathbf{R}_z$ is the rotation matrix about the z-axis.

B. CTR performance metrics

In order to evaluate the different CTR architectures, performance metrics are needed to quantitatively compare the advantages and disadvantages of each robot design. The commonly used CTR performance metrics include: 1) workspace, 2) orientability, 3) stability, and 4) dexterity. Previous studies often include only a subset of these metrics to assess a particular CTR design. Here we evaluate all of the above metrics using the following workflow (see Fig. 2).

For a given CTR design, a set of 50,000 configurations is computed by solving Eq. 1 and Eq. 2. 40,000 of these configurations are computed based on sampling the joint space, where only stable configurations are considered. The other 10,000 points are randomly sampled with aligned and opposite rotations in order to compute the stability metric, as explained in Section II-B.3. The unstable configurations are removed from the set, such that only the stable configurations are considered in the computation of the workspace volume,

orientability, and dexterity. Under the assumption of cylindrical symmetry, each configuration is rotated about the z-axis, such that the tip positions of all configurations lie in the same plane, as shown in pink in Fig. 2(a). These configurations are then used to compute the workspace size, orientability, and dexterity, as shown in Fig. 2(b) and Fig. 2(c), and described in detail below.

1) Workspace volume: The versatility of a CTR is impacted by its reachable volume, where a higher value represents a larger number of reachable locations where a given CTR can perform surgical tasks. With the end points of each configuration rotated onto the same plane, the planar workspace boundary is formed using the *boundary* function in MATLAB, as shown in Fig. 2(b). The area within the boundary is considered reachable by the CTR. Under the assumption of cylindrical symmetry, the volume of the CTR is computed by integrating the 2D workspace boundary about the z-axis.

2) Orientability: Orientability defines the ability of a CTR to reach the same endpoint from different angles, which can be important during surgical procedures. To compute orientability, the CTR workspace slice shown in Fig. 2(b) is discretized into 3 mm by 3 mm square regions. Using the method proposed in [19], a service sphere, with the north pole restricted to the positive z-direction of the base, is formed to encompass each square region, illustrated in Fig. 2(c). Each service sphere is discretized along the longitudinal and lateral axes into patches of equal surface area, with each patch representing a possible orientation. The area of the patches representing achievable orientations (shown in green in Fig. 2(c)) is divided by the total surface area of the service sphere to obtain the local orientability for each square region. Local orientability ranges from 0 to 1, with 1 indicating that the corresponding square region is reachable by the robot in all orientations [19]. The global orientability is computed as the average of all local orientability values.

3) Stability: When tubes have overlapping opposite or aligned curvatures, a CTR can experience instabilities, where there exists multiple solutions to the forward kinematics model. The robot can suddenly snap from one stable configuration to another [20], and it is typically best to avoid such uncontrollable motions. In order to evaluate the stability, the relative tube angle at the equilibria needs to be considered and can be defined as θ_e. The local bifurcation approach is used and considered at the equilibria where $\theta_e = 0, \pi$. The propagation of linearized solutions from the base to the tip of the robot is processed to find the bifurcation points and can be described as follows [20]:

$$\dot{\theta}(L_i + \beta_i) = S_2 \dot{\theta}(0) \tag{3}$$

where $\theta_i = \psi_i - \psi_1$ and S_2 is the $(n-1) \times (n-1)$ square matrix that describes the kinematic solutions in each section of the robot [20]. The stability criterion, $\det(S_2) \leq 0$, indicates the equilibrium configuration has bifurcated and the robot becomes unstable.

4) Dexterity: Local dexterity is a common approach that is used for characterizing the robot's ability to move or apply force in any direction [21]. High dexterity is often critical for many medical interventions due to the complexity of surgical tasks that must be performed inside highly constrained environments. One common measure for the dexterity index is to look at the condition number, c, of the smallest and largest eigenvalues of the end-effector Jacobian, J [22], [23]. The Jacobian matrix can be expressed as $J(\theta) = \begin{bmatrix} J_w(\theta) & J_v(\theta) \end{bmatrix}^T$, and is divided into linear velocity (J_v) and angular velocity (J_w) terms. The global dexterity measures are described as follows [21]:

$$\begin{aligned} D_w &= \frac{\sum_{i=0}^{N} c_{wi}}{N}, c_w = \frac{\lambda_{min}(A_w)}{\lambda_{max}(A_w)}, \\ D_v &= \frac{\sum_{i=0}^{N} c_{vi}}{N}, c_v = \frac{\lambda_{min}(A_v)}{\lambda_{max}(A_v)}, \end{aligned} \tag{4}$$

where c_w and c_v are the local dexterity measures, which also refer to the inverse of the condition number, and whose values are between [0, 1]. $\lambda(A_w)$ and $\lambda(A_v)$ are the eigenvalues of matrix A_w and A_v, respectively, where $A_w = J_w J_w^T$, $A_v = J_v J_v^T$, and N is the number of points in the sampled workspace.

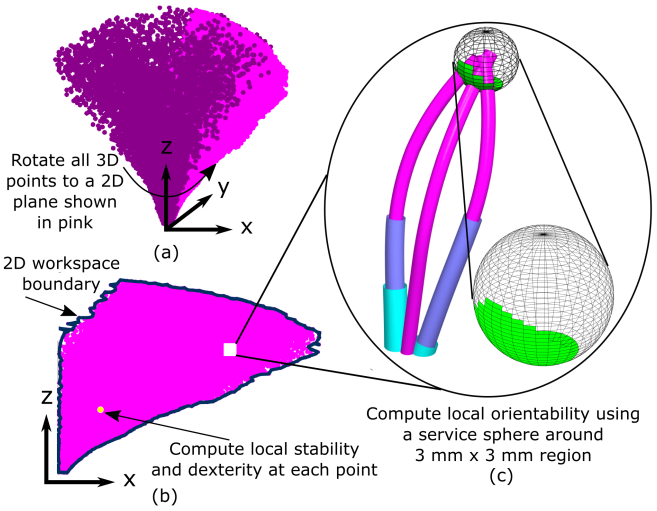

Fig. 2. (a) To compute the CTR performance metrics, the set of tip positions resulting from joint sampling (purple) are rotated about the z-axis into a single plane (pink). (b) Local metrics, including stability and dexterity, are then computed at every point. (c) Local orientability is computed for discretized 3x3 mm regions by assessing the achievable orientations, represented by the green patches of a surrounding service sphere. Local orientability and dexterity are then averaged across the entire workspace, and global stability is computed as a percent of stable configurations over all configurations .

III. CTR PERFORMANCE ANALYSIS

Two simulation studies are performed to understand the advantages and disadvantages of the different CTR architectures. The first study compares the performance among each of the architectures using three-tube CTRs. The second study is designed to show that with the proposed architectures, fewer tubes can be used to achieve similar performance to that using a three-tube, single constant-curvature CTR.

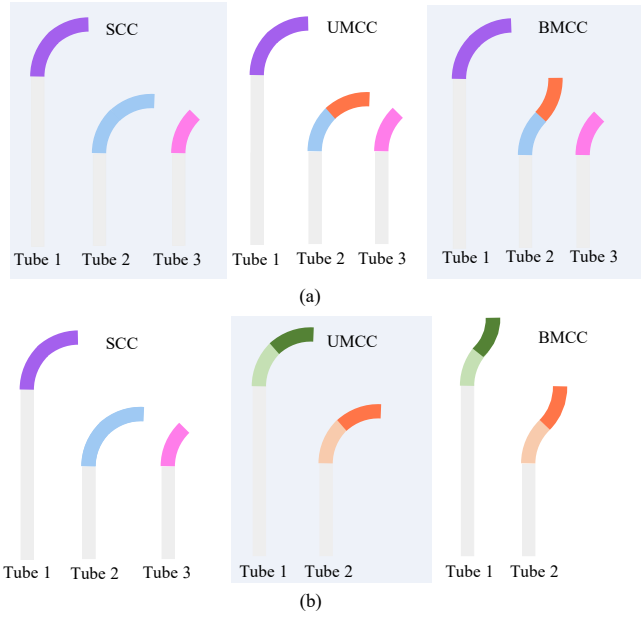

Fig. 3. (a) Tube sets used for study 1, where tube 1 and tube 3 remain constant for all three architectures. The curvature of the distal curved section of the UMCC and BMCC designs (shown in orange) are varied and the effects on each performance metric are compared. (b) Tube sets used for study 2, where the same standard three-tube CTR is used. The curvatures of two-tube UMCC and BMCC sets are varied in order to determine whether any two-tube set can achieve similar performance across all metrics compared to the standard three-tube single constant-curvature design.

A. Simulation setup

CTR performance highly depends on the tube design parameters, including tube diameter, material properties, tube length, and tube pre-curvature. Given the large design space, it is not straightforward to compare the performance between architectures without constraining the number of variables. Therefore, all tube sets have the same pre-selected tube diameters and are made from the same material (Nylon 12, Duke Extrusion). The tube diameters are selected to be small enough for minimally invasive procedures, and to ensure variable curvature sections with balanced-stiffness. The average tube clearance is 0.15 mm, which is comparable to standard Nitinol tube sets. Table I shows the tube parameters used for the simulation study, with the parameters common across all sets provided in the caption.

B. Study design

1) Study 1: We start by comparing three, three-tube CTRs by examining the trends in the performance metrics as the curvature of the distal end of the curved section of one of the MCC tubes is varied. To ensure a fair comparison between architectures, the length of the straight section and curved section for the ith tube remain constant. In addition, the design of tube 1 and tube 3 remain fixed across architectures. Previous studies have shown that a variable curvature section close to the proximal end of a CTR can improve the workspace and orientability [24]. Therefore, tube 2 is chosen to be constructed with different architectures in order to create variable curvature sections when combined with tube 3. Here we divide the curved section into two subsections of equal length. The curvature of the proximal subsection matches the curvature of the SCC tube 2, as shown in blue in Fig. 3(a). The curvature of the distal subsection, shown in orange in Fig. 3(a), is varied from low curvature to high curvature in order to observe the general trend of using these different architectures. For UMCC tubes, the curvature of the proximal and distal subsections are in the same direction, and for BMCC tubes, they are in opposite directions.

2) Study 2: The goal of the second study is to investigate whether a smaller number of tubes can be used to obtain similar performance to that of a three-tube, standard CTR. Although CTRs with fewer tubes have a lower number of degrees of freedom, they also require fewer actuators, which can reduce system complexity and cost. Therefore, if an MCC CTR with fewer tubes can still achieve similar performance in terms of the proposed metrics, there could be a substantial overall benefit in selecting such a design. A three-tube SCC CTR with parameters shown in Table I is used. The UMCC and BMCC designs both consist of only two tubes, where both tube 1 and tube 2 have multiple constant curvatures, as shown in Fig. 3(b). The length of the straight and curved sections of the MCC designs remain the same as the SCC design for tube 1 and tube 2. The difference is that the curved section of the MCC designs is divided into two subsections of equal length, whose curvature values are randomly selected from a set of 9 curvatures that are evenly spaced between the curvature range given in Table I. A total of 50 UMCC tube sets and 50 BMCC tube sets were randomly selected for this study.

C. Results

1) Study 1 Results: The results of study 1 are shown in the spider plots in Fig. 4. These plots show the metrics that were discussed in Section II. B, including the workspace, dexterity in translation and rotation, stability, and orientability, and help to visualize the general trends. Focusing first on the comparison between the SCC and UMCC designs, we can see that increasing the curvature of the distal end of tube

TABLE I

TUBE DESIGN PARAMETERS. FOR ALL SETS, THE FOLLOWING REMAIN CONSTANT: $OD_1 = 1.98$ MM, $ID_1 = 1.47$ MM, $OD_2 = 2.64$ MM, $ID_2 = 2.13$ MM, $OD_3 = 3.3$ MM, $ID_3 = 2.79$ MM, $L_{s1} = 167$ MM, $L_{s2} = 61$ MM, $L_{s3} = 45$ MM, $E = 1.45$ GPA, $G = 0.5205$ GPA.

	SCC			UMCC		BMCC	
Tube #	1	2	3	1	2	1	2
Study 1							
r_1 [mm]	39	54	100	39	54	39	54
L_{c1} [mm]	30	60	30	30	30	30	30
r_2 [mm]	x	x	x	x	[135, 34]	x	[135*, 34*]
L_{c2} [mm]	x	x	x	x	30	x	30
Study 2							
r_1 [mm]	78	108	200	[385, 44]	[526, 60]	[385, 44]	[526, 60]
L_{c1} [mm]	30	60	30	15	30	15	30
r_2[mm]	x	x	x	[385, 44]	[1000, 111]	[385*, 44*]	[1000*, 111*]
L_{c2} [mm]	x	x	x	15	30	15	30

* indicates a negative radius of curvature (-x direction),
[ ] indicates the range of radii,
Note: For study 1, tube 3 for the MCC sets is identical to the SCC tube 3.

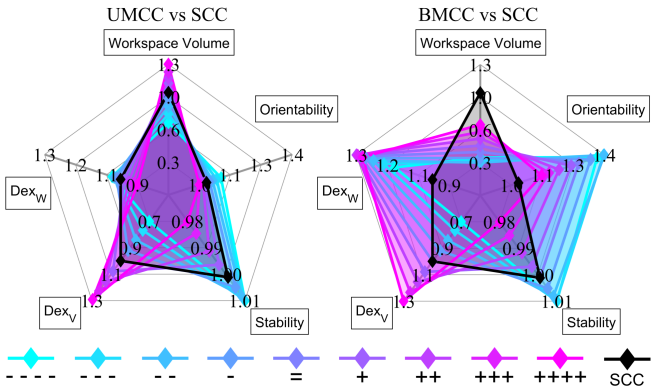

Fig. 4. Spider plots showing results from study 1. Five metrics are shown for the UMCC and BMCC architectures and are compared to those of an SCC CTR, shown in black. Each value is scaled by dividing by the corresponding value of the SCC tube set. The distal curved section of tube 2 of the UMCC and BMCC CTR is varied, where each "+", represents a 15% increase in curvature from the SCC design and each "-", represents a 15% decrease.

2, results in a larger workspace and increased dexterity in translation. We can also see that there seems to be little effect on the orientability, however, increasing the curvature does result in decreased stability. Decreasing the curvature of the distal end of tube 2 significantly reduces the overall workspace and dexterity in translation. In contrast, the three-tube BMCC design results in a smaller workspace regardless of curvature because the tip of the tube curves back towards the z-axis of the robot base. Nonetheless, the overall orientability and dexterity increase and are higher than the other two designs (SCC, UMCC). Both UMCC and BMCC designs show a decrease in stability when the curvature increases.

2) Study 2 Results: In order to determine whether a two-tube CTR can achieve similar or better performance using tubes with multiple constant curvature, all MCC tube sets that achieve a higher value than the SCC tube set in at least four metrics are identified. From this set, three UMCC tube sets and three BMCC tube sets are manually selected and shown in Fig. 5. As seen in Fig. 5, there are multiple two-tube UMCC tube sets that can achieve similar performance to the SCC set, and some of these sets even have improved dexterity and orientability. Looking at the shape of the workspace for these UMCC tube sets, we see that although the overall size of the workspace is comparable to that of the three-tube SCC CTR, the center region appears to be less reachable. However, depending on the particular task, such a tradeoff may be reasonable. As expected from study 1, it is clear that the BMCC designs that perform comparably to a three-tube SCC set in terms of dexterity, orientability, and stability, result in significantly smaller workspaces. However, as seen in the worksplace plot in Fig. 5, a BMCC design can enable better coverage in the center region that can be difficult to reach. Overall, the results suggest that it is possible to design two-tube CTRs with multiple constant curvatures that can achieve similar performance to a standard SCC tube set, at least across a subset of the performance metrics evaluated. The tradeoffs among the architectures in terms of the various performance metrics must be considered based on the particular application.

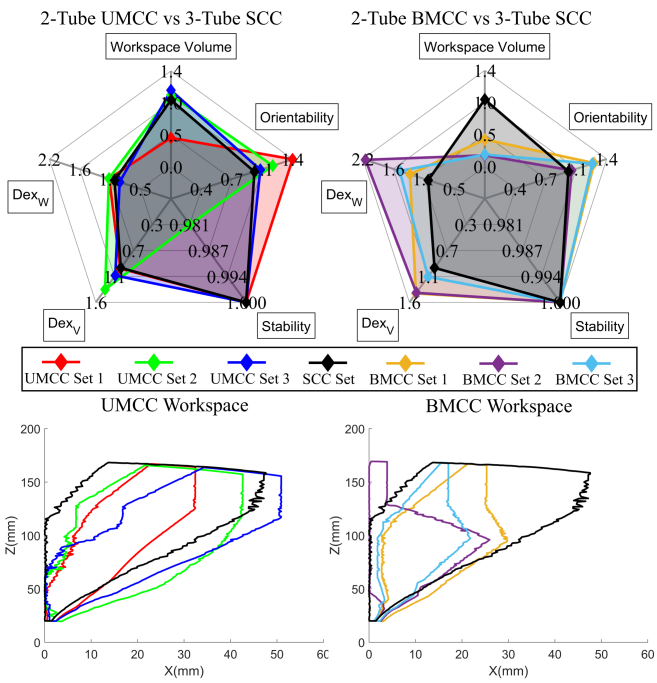

Fig. 5. Three two-tube UMCC sets (red, green, blue) and three two-tube BMCC sets (yellow, purple, cyan) with an improvement in four out of the five metrics compared to a three-tube SCC set. (top) Spider plots illustrating the performance metrics of a two-tube UMCC set, a two-tube BMCC set, and a three-tube SCC set. Each value is scaled by dividing by the corresponding value of the SCC tube set. (bottom) The boundary of the workspace slice of the two-tube MCC sets and the three-tube SCC set are plotted to visualize the difference in the shape of the workspaces.

IV. HARDWARE VALIDATION

In this section, we present the first hardware demonstration of CTRs using the UMCC and BMCC architectures. We first present our process for heat-setting the tubes into the desired pre-curved shapes. We then fabricate three different tube sets based on the previously presented simulations. Finally, we experimentally measure the workspace of these CTRs and compare the results to those obtained in simulation.

A. Fabrication

To date, the proposed method for heat setting nylon tubes involves the use of a heat gun and a jig with the desired shape. Building on this previous work, we investigated numerous approaches to both heat application and jig creation. We found that in order to obtain accurate and repeatable results, it was important to ensure consistent heating across the entire tube at a controllable temperature with immediate cooling of the tube. Specifically, we found that the use of a heat gun and a 1-sided jig made it challenging to apply a consistent level of heat across the entire tube. Results varied quite significantly based on the distance between the heat gun and the tube, and for longer sections, it was difficult to properly heat the entire section at the same time. This resulted in inconsistent cross sections, inconsistent springback along the tube, and a need for skill when using a heat gun. We found that the use of an oven, combined with a jig that exposes a large portion of the tube to direct heat,

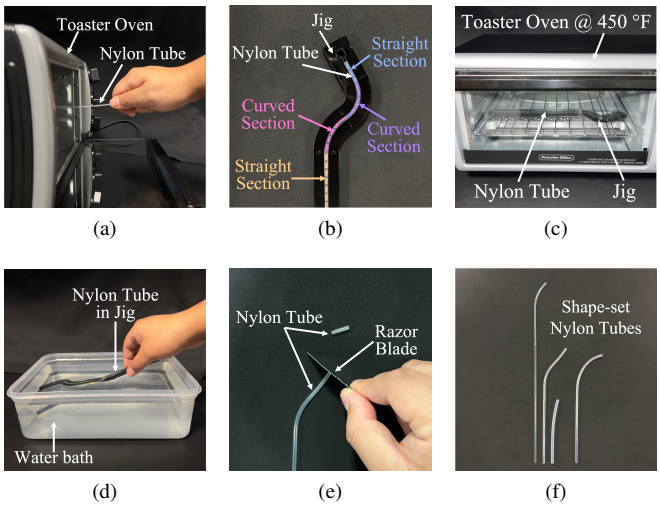

Fig. 6. Fabrication steps are as follows: (a) preheat the tube at 450°F for 10 seconds, (b) place the tube into the jig, (c) heat at 450°F for 55 seconds, (d) quench in water bath immediately and run under cold water for 90 seconds, (e) cut off the extra straight section of the tube, and (f) tubes are complete.

enables even and controllable heating across the tube while maintaining its cross section.

Based on these initial tests, we used the following protocol (Fig. 6). First, jigs are made by laser cutting 1/4" acrylic into the desired shape. Next, the oven is set to 450°F. With the oven door left open, the section of the tube to be curved is then held inside for 10 seconds. The Nylon tube is then immediately placed into the jig and allowed to cool for 60 seconds. The jig is then placed inside the oven (still set to 450°F), and the door is closed for 55 seconds. The jig is then immediately placed inside a water bath to cool, and run under cold water for 90 seconds. Once cool, the distal end of the curved section is marked and and cut with a razor blade.

B. Experimental setup

We begin by fabricating one UMCC tube set and one BMCC tube set (Table II). To highlight the differences between the proposed MCC architectures, the sets selected represent the curvatures at both extremes collected from study 1. After heat-setting, the tubes are translated 20 times through a straight rod to overcome the most significant effects of fatigue [16]. The final tube curvatures are then measured and are given in Table II. The tubes are then assembled and attached to the actuation unit presented in [25] (Fig. 7). An electromagnetic (EM) sensor is attached to the tip of the CTR, and an Aurora EM tracking system (NDI) is used to measure its 3-D position.

TABLE II

MEASURED TUBE RADIUS OF CURVATURE

Study 1	UMCC			BMCC		
	Tube 1	Tube 2	Tube 3	Tube 1	Tube 2	Tube 3
r_1 [mm]	40	50	127	40	48	94
r_2 [mm]	40	44	127	40	141*	94

* indicates a negative radius of curvature (-x direction)

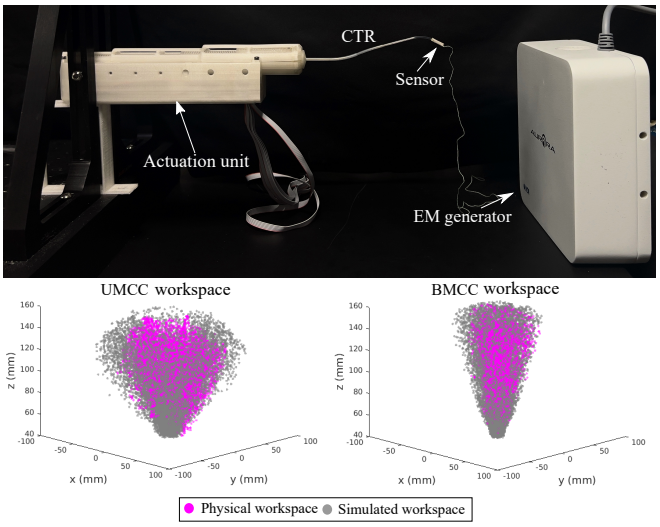

Fig. 7. (a) Experimental setup, including actuation system, assembled CTR, and EM tracking system. (b) Measured workspace for a UMCC and an BMCC CTR (pink), overlaid with the simulated workspace (grey).

C. Hardware demonstration

To demonstrate the feasibility of using physical UMCC and BMCC tubes, the following workspace measurements are performed. Each CTR is actuated using a set of 13000 randomly sampled joint values and the tip positions are recorded. The results are plotted in pink in Fig. 7, along with the simulated workspace (in grey), as computed using the measured curvature values. For both architectures, the general shape of the physically measured workspace matches well with that of the simulated workspace, but the size of the physical workspace is slightly smaller. This discrepancy could be due to effects such as friction and tube clearance, which are not taken into account in the model, or could be due to fatigue of the tubes, which can cause a decrease in the tube curvature. We also note that the geometry of the BMCC tubes are more difficult to translate and rotate relative to each other compared to other tube architectures due to increased friction. The results highlight the differences in one performance metric that result from using different tube architectures and confirm the simulated results.

V. CONCLUSION

In this paper, we designed, fabricated, and validated three-tube, fully Nylon CTRs with multiple constant-curvature tubes. A simulation study was conducted to evaluate the performance of the proposed tube architectures in terms of several metrics, including workspace volume, orientability, stability, and dexterity. The study shows that compared to using standard single constant-curvature tubes, using tubes with multiple constant curvatures can lead to an improvement in several performance metrics, but often at the cost of a decrease in the performance in others. Depending on the particular application, the tradeoffs should be considered when selecting the best tube architecture to use.

REFERENCES

[1] P. Sears and P. Dupont, "A steerable needle technology using curved concentric tubes," in *IEEE/RSJ Int. Conf. on Intelligent Robots and Systems*, 2006, pp. 2850–2856.

[2] R. J. Webster, A. M. Okamura, and N. J. Cowan, "Toward active cannulas: Miniature snake-like surgical robots," in *IEEE/RSJ Int. Conf. on Intelligent Robots and Systems*, 2006, pp. 2857–2863.

[3] T. L. Bruns, A. A. Remirez, M. A. Emerson, R. A. Lathrop, A. W. Mahoney, H. B. Gilbert, C. L. Liu, P. T. Russell, R. F. Labadie, K. D. Weaver *et al.*, "A modular, multi-arm concentric tube robot system with application to transnasal surgery for orbital tumors," *Int. Journal of Robotics Research*, vol. 40, no. 2-3, pp. 521–533, 2021.

[4] H. Alfalahi, F. Renda, and C. Stefanini, "Concentric tube robots for minimally invasive surgery: Current applications and future opportunities," *IEEE Trans. on Medical Robotics and Bionics*, vol. 2, no. 3, pp. 410–424, 2020.

[5] C. Bergeles, A. H. Gosline, N. V. Vasilyev, P. J. Codd, J. Pedro, and P. E. Dupont, "Concentric tube robot design and optimization based on task and anatomical constraints," *IEEE Trans. on Robotics*, vol. 31, no. 1, pp. 67–84, 2015.

[6] Q. Peyron, Q. Boehler, P. Rougeot, P. Roux, B. J. Nelson, N. Andreff, K. Rabenorosoa, and P. Renaud, "Magnetic concentric tube robots: introduction and analysis," *Int. Journal of Robotics Research*, vol. 41, no. 4, pp. 418–440, 2022.

[7] M. T. Chikhaoui, K. Rabenorosoa, and N. Andreff, "Kinematics and performance analysis of a novel concentric tube robotic structure with embedded soft micro-actuation," *Mechanism and Machine Theory*, vol. 104, pp. 234–254, 2016.

[8] D.-Y. Lee, J. Kim, J.-S. Kim, C. Baek, G. Noh, D.-N. Kim, K. Kim, S. Kang, and K.-J. Cho, "Anisotropic patterning to reduce instability of concentric-tube robots," *IEEE Transactions on Robotics*, vol. 31, no. 6, pp. 1311–1323, 2015.

[9] J. Ha and P. E. Dupont, "Designing stable concentric tube robots using piecewise straight tubes," *IEEE Robotics and Automation Letters*, vol. 2, no. 1, pp. 298–304, 2016.

[10] J. Ha, F. C. Park, and P. E. Dupont, "Optimizing tube precurvature to enhance the elastic stability of concentric tube robots," *IEEE Transactions on Robotics*, vol. 33, no. 1, pp. 22–37, 2016.

[11] N. Morgan and M. Broadley, "Taking the art out of smart!-forming processes and durability issues for the application of niti shape memory alloys in medical devices," *Materials and Processes for Medical Devices Coference*, pp. 247–252, 2004.

[12] S. Smith and E. Hodgson, "Shape setting nitinol," in *Materials and Processes for Medical Devices Conference*, 2004, pp. 266–270.

[13] H. B. Gilbert and R. J. Webster, "Rapid, reliable shape setting of superelastic nitinol for prototyping robots," *IEEE Robotics and Automation Letters*, vol. 1, no. 1, pp. 98–105, 2015.

[14] T. K. Morimoto and A. M. Okamura, "Design of 3-D printed concentric tube robots," *IEEE Trans. on Robotics*, vol. 32, no. 6, pp. 1419–1430, 2016.

[15] E. Amanov, T.-D. Nguyen, and J. Burgner-Kahrs, "Additive manufacturing of patient-specific tubular continuum manipulators," in *Medical Imaging 2015: Image-Guided Procedures, Robotic Interventions, and Modeling*, vol. 9415. SPIE, 2015, pp. 420–428.

[16] G. Noh, S. Y. Yoon, S. Yoon, K. Kim, W. Lee, S. Kang, and D. Lee, "Expeditious design optimization of a concentric tube robot with a heat-shrink plastic tube," in *IEEE/RSJ Int. Conf. on Intelligent Robots and Systems*, 2016, pp. 3671–3676.

[17] A. L. Gunderman, S. Sengupta, E. Siampli, D. Sigounas, C. Kellner, C. Oluigbo, K. Sharma, I. Godage, K. Cleary, and Y. Chen, "A surgical platform for intracerebral hemorrhage robotic evacuation (ASPIHRE): A non-metallic mr-guided concentric tube robot," *arXiv preprint arXiv:2206.09848*, 2022.

[18] D. C. Rucker, R. J. Webster III, G. S. Chirikjian, and N. J. Cowan, "Equilibrium conformations of concentric-tube continuum robots," *Int. Journal of Robotics Research*, vol. 29, no. 10, pp. 1263–1280, 2010.

[19] L. Wu, R. Crawford, and J. Roberts, "Dexterity analysis of three 6-dof continuum robots combining concentric tube mechanisms and cable-driven mechanisms," *IEEE Robotics and Automation Letters*, vol. 2, no. 2, pp. 514–521, 2017.

[20] R. J. Hendrick, H. B. Gilbert, and R. J. Webster, "Designing snap-free concentric tube robots: A local bifurcation approach," in *IEEE Int. Conf. on Robotics and Automation*, 2015, pp. 2256–2263.

[21] F. C. Park and R. W. Brockett, "Kinematic dexterity of robotic mechanisms," *The International Journal of Robotics Research*, vol. 13, no. 1, pp. 1–15, 1994.

[22] K. M. Lynch and F. C. Park, *Modern robotics*. Cambridge University Press, 2017.

[23] K. Leibrandt, C. Bergeles, and G.-Z. Yang, "Implicit active constraints for concentric tube robots based on analysis of the safe and dexterous workspace," in *2017 IEEE/RSJ International Conference on Intelligent Robots and Systems (IROS)*. IEEE, 2017, pp. 193–200.

[24] P. E. Dupont, J. Lock, B. Itkowitz, and E. Butler, "Design and control of concentric-tube robots," *IEEE Trans. on Robotics*, vol. 26, no. 2, pp. 209–225, 2009.

[25] C. Girerd and T. K. Morimoto, "Design and control of a hand-held concentric tube robot for minimally invasive surgery," *IEEE Trans. on Robotics*, vol. 37, no. 4, pp. 1022–1038, 2020.